Int Ophthalmol (2019) 39:2709–2719
https://doi.org/10.1007/s10792-019-01115-7

ORIGINAL PAPER

Swept source-OCT and swept source-OCT angiography findings in posterior microphthalmos

Nesrine Abroug · Imen Ksiaa · Marco Lupidi · Wejdene Nabi · Sonia Attia · Bechir Jelliti · Sana Khochtali · Moncef Khairallah

Received: 20 December 2018 / Accepted: 30 April 2019 / Published online: 10 May 2019

Abstract

Purpose To describe swept source-OCT (SS-OCT) and swept source-OCT angiography (SS-OCTA) findings in eyes with posterior microphthalmos (PM).

Methods Twelve eyes (six patients) with PM were evaluated using SS-OCT and SS-OCTA. Structural changes, subfoveal choroidal thickness (SFCT), and perifoveal capillary changes with qualitative and quantitative assessments were analyzed. Twenty eyes served as control group.

Results SS-OCT findings included elevated retinal papillo-macular fold (75%), retinal pigment epithelium folds (83%), macular cystoid spaces (42%), subretinal fluid (17%), and increased visibility of posterior vitreous cortex and hyaloid (42%). Mean SFCT in PM and in control eyes were 430.33 ± 157.48 µm and 290.05 ± 52.87 µm, respectively ($p = 0.004$). Perifoveal capillary changes on SS-OCTA included foveal avascular zone (FAZ) remodeling (100%), vessel tortuosity (67%), disorganization of the deep capillary network (67%), intraretinal cystoid spaces (42%), and areas of signal voids in the choriocapillaris (33%). FAZ area was significantly smaller in eyes with PM than in the control group in both the superficial ($p < 0.001$) and deep capillary plexuses ($p = 0.001$). Capillary vessel density (CVD) was significantly lower in the PM than in the control group in the deep capillary plexus ($p = 0.004$). Log MAR BCVA correlated negatively with axial length ($r = -0.929$, $p < 0.001$), FAZ area in both the superficial ($r = -0.637$, $p < 0.001$) and deep capillary plexus ($r = -0.561$, $p = 0002$), and CVD in the deep capillary plexus ($r = -0.450$, $p = 0.016$).

Conclusions Combined SS-OCT and SS-OCTA allow the detection of various retinal and choroidal structural and microvascular changes in eyes with PM. These findings can provide new insights onto this blinding ocular condition.

Keywords Fovea · Optical coherence tomography · Optical coherence tomography angiography · Posterior microphthalmos · Swept source

N. Abroug · I. Ksiaa · W. Nabi · S. Attia · B. Jelliti · S. Khochtali · M. Khairallah (✉)
Department of Ophthalmology, Fattouma Bourguiba University Hospital, Faculty of Medicine, University of Monastir, 5019 Monastir, Tunisia
e-mail: moncef.khairallah@rns.tn

M. Lupidi
Section of Ophthalmology, Department of Surgical and Biomedical Sciences, University of Perugia, S. Maria della Misericordia Hospital, 06156 Perugia, Italy

Introduction

Posterior microphthalmos (PM) is an autosomal recessive ocular condition characterized by high

hyperopia, posterior segment foreshortening with a total axial length (AL) more than two standard deviations smaller than the normal for that age group, and normal aspect of the anterior segment with normal or subnormal dimensions without other major ocular or systemic anomalies [1, 2]. An elevated retinal papillo-macular fold (RPMF) is a characteristic finding in most eyes with this condition [1, 3]. A wide variety of other pathologic features of eyes with PM have been described using B-scan ultrasonography (USG), fluorescein angiography (FA), and spectral domain optical coherence tomography (SD-OCT) [3–10]. These include absence of the capillary-free zone, retinal wrinkles, macular cystoid spaces, pigmentary retinopathy, chorioretinal folds, uveal effusion, sclerochoroidal thickening, crowded optic disk, absence of a foveal depression, increased posterior pole curvature, which is correlated with both RPMF height and inverse AL, and an omega- or dome-shaped retinal fold [3–10].

Swept source-OCT (SS-OCT) is a recent advance in retinal and choroidal imaging. It is characterized by a fast scanning speed over a wide area, coupled with a high axial resolution. In addition, it provides a uniform sensitivity over the entire scanning volume, allowing a high-quality simultaneous imaging of the vitreous, retina, and choroid.

Optical coherence tomography angiography (OCTA) is a recently developed, label-free, imaging modality that provides high-resolution, En face images of the retinal and choroidal microvasculature. It has enabled clinicians to investigate in vivo the retinal and choroidal vascular perfusion with a depth-resolved approach. OCTA has already shown itself to be clinically useful in evaluating foveal microvascular changes in numerous retinal and choroidal conditions including diabetic retinopathy, retinal vascular occlusions, sickle cell disease, macular telangiectasia, paracentral acute middle maculopathy, choroidal neovascularization, and inflammatory conditions [11–13].

To the best of our knowledge, eyes with PM have not been previously evaluated by SS-OCT or SS-OCTA. The purpose of this study was to describe the posterior segment changes in patients with PM using these novel imaging modalities.

Methods

This was a comparative case series of 12 eyes of six patients diagnosed with PM at the department of Ophthalmology, Fattouma Bourguiba University Hospital of Monastir, Tunisia.

The study protocol was approved by the ethics committee of our institution (Fattouma Bourguiba University Hospital IEC), and the research followed the tenets of the Declaration of Helsinki. All patients provided informed consent for participation before being included in the study.

The diagnostic criteria of PM were the presence of high hyperopia, a marked foreshortening of the posterior segment with normal or slightly smaller than normal anterior segment dimensions, and no other ocular malformations or associated syndromic disease. All identified PM patients underwent a detailed ophthalmic examination including measurement of Snellen best-corrected visual acuity (BCVA), cycloplegic refraction, slit-lamp examination, tonometry, dilated fundus examination with noncontact or contact lenses, and A-mode and B-mode USG.

Twenty age- and gender-matched healthy subjects served as controls.

SS-OCT and OCTA (DRI OCT Triton plus, Topcon, Tokyo, Japan) were performed for all patients. This system uses a short cavity swept laser with longer wavelength of operation (1050 nm) and a speed of 100,000 A-scans per seconds. All OCT and OCTA scans were obtained by the same experienced operator (NA). A three-dimensional (3D) 12 mm × 9 mm scan and/or a 12-mm radial macular scan made of 12 line scans spread across 360° were obtained. Subfoveal choroidal thickness (SFCT) was measured as the perpendicular distance from the outer portion of the hyperreflective line of the retinal pigment epithelium (RPE)–Bruch's membrane interface to the hyperreflective line of the sclerochoroidal interface using the manual caliper function in the SS-OCT software (Fig. 1). Two measurements were obtained from the vertical and horizontal sections under the center of the fovea from OCT data by two experienced observers (NA, IK) and were averaged for analysis.

Three-dimensional OCT angiograms were acquired over a 6 × 6 mm and 3 × 3 mm field of view and generated by the built-in software (IMAGEnet6). Preset parameters were used to segment the capillary bed in the superficial capillary plexus (SCP), deep

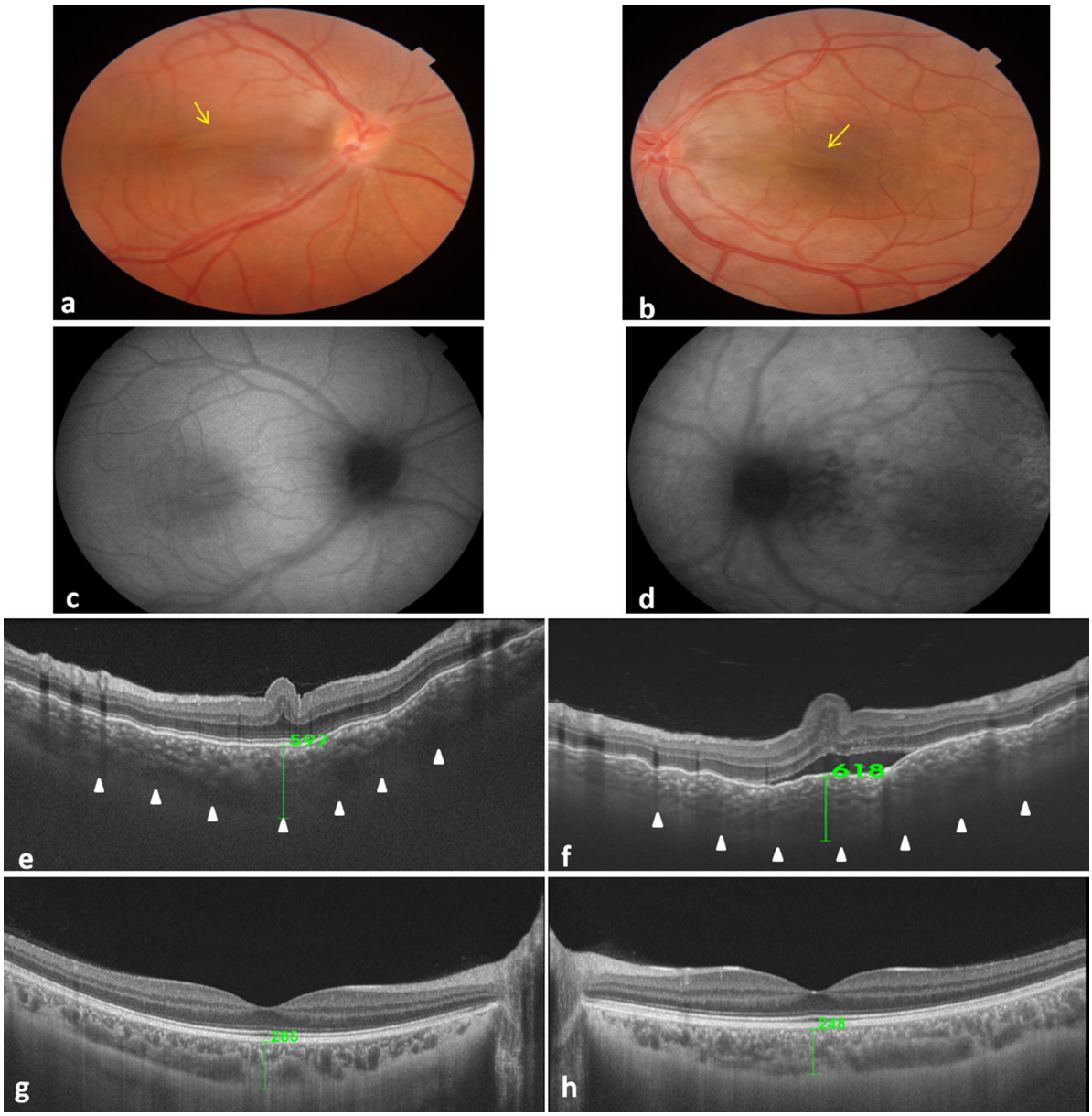

Fig. 1 Measurement of subfoveal choroidal thickness (SFCT) using SS-OCT in patient 6. Color fundus photographs OU show an elevated PMF and a crowded optic disk (**a**, **b**). Fundus autofluorescence shows multiple hypoautofluorescent areas in the posterior pole in the LE (**c**, **d**).Vertical SS-OCT sections show the dome-shaped RPMF with fine retinal surface wrinkles, and RPE folds OU (**e**, **f**). Subretinal fluid and marked RPE folds secondary to uveal effusion are seen in the LE (**f**). The SFCT was manually measured at the fovea and defined as the vertical distance between the RPE line and the hyper-reflective line behind the large choroidal vessel layers, presumed to be the sclerochoroidal interface (white arrowheads). The SFCT was markedly thicker in the PM patient than in the age-matched subject (**g**, **h**)

capillary plexus (DCP), outer retina, and choriocapillaris (CC). Poor-quality OCT angiograms including signal loss due to blinking or fixation loss, quality score of below 40, motion artifacts, or inaccurate segmentation of tissue layers or slabs were excluded from the evaluation.

Original OCTA images were exported in jpg format to be analyzed by two independent masked examiners (NA and IK). The 3 × 3 OCT angiograms were

evaluated for the following characteristics: foveal avascular zone (FAZ) area, FAZ remodeling (including asymmetry of the FAZ due to a ragged or punched-out border, irregularities or disruption of the FAZ outlines, or loss of the normal architecture of capillaries in the perifoveal area), perifoveal capillary changes (including capillary dilatation, tortuosity, telangiectasia, shunting vessels, and areas of rarefied capillaries), areas of capillary hypoperfusion/non-perfusion (presenting as irregular hypo intense greyish areas), disorganization of the superficial and deep capillary network (defined as localized or diffuse loss of the normal architecture of the capillary network), intraretinal cystoid spaces (presenting as well-defined black roundish areas without any signal on OCTA), and areas of signal voids in the CC. The 6 × 6 mm OCT angiograms were used as an adjunct to the 3 × 3 mm OCT angiogram to provide an assessment on a wider scanning field. In instances of disagreement, there was open adjudication between the two readers until a consensus was established.

FAZ area measurements were performed using the Fiji software (an expanded version of ImageJ version 1.51a, available at fiji.sc/). The FAZ area was manually outlined using the image scaling and caliper tool set included in Fiji. The measurements were averaged to obtain a final value and were compared with those measured in healthy, age-matched, control subjects.

In the capillary vessel density (CVD) analysis, the original OCTA images of the SCP and DCP were binarized and then skeletonized using the Fiji software. CVD was calculated as the number of white pixels over the total number of pixel. To measure the CVD in the CC, a binarization of the original images was done using the Otsu method, which is an automatic threshold selection from gray-level histograms (Fig. 2). The thresholded images were then analyzed with the "Analyze Particles" command, and the CC vascular flow area was defined as the percentage of the white pixels against the whole scan area [14, 15].

Statistical analyses were performed using SPSS software version 21 (SPSS, Inc., Chicago, Illinois, USA). Descriptive statistics (percentages, means, and standard deviation) were computed for demographic and clinical variables. BCVA was converted to the logarithm of the minimum angle resolution (log MAR) for statistical evaluation. Mann–Whitney test was used for nonparametric quantitative data analysis, and Pearson's r correlation was used to examine the relationships among the measured variables. Statistical significance was set at $p < 0.05$.

Results

Six patients were enrolled in the current study (3 females and 3 males), and the mean age was 42.16 ± 14.45 years (range 25–64; median 43). The mean age of the control group was 46.6 ± 16.36. The mean age and gender distribution were not significantly different between the two groups ($p = 0.413$ and $p = 0.787$, respectively) (Table 1).

All enrolled patients had bilateral high hyperopia ranging from + 13 to + 18.75 *D* (mean 16.08 ± 1.8 *D*) with bilateral foreshortening of the posterior ocular segment (mean AL 15.91 ± 0.50 mm; range 15.1–16.83 mm) with associated normal or slightly smaller than normal anterior segment dimensions. The BCVA ranged from 20/400 to 20/63 (mean 20/125) Snellen equivalents. Intraocular pressure was normal in all eyes (range 12–18; median 14). No other systemic abnormalities involving physical or mental development were noted. The demographic and ocular features of patients are listed in Table 2.

Fundus examination showed a bilateral elevated RPMF in 9/12 eyes (75%). This was horizontal in five of the nine eyes and oblique with inferior displacement of the fovea and retinal vessels in four eyes. Other posterior segment changes included fine retinal folds ($n = 3$ eyes; 25%), chorioretinal folds ($n = 4$ eyes; 33%), visible retinal cystoid spaces within the RPMF ($n = 3$ eyes; 25%), retinal pigmentary changes ($n = 4$ eyes; 33%), and crowded optic disks ($n = 12$ eyes; 100%). Clinically evident uveal effusion was noted in two eyes (patients 3 and 6), and it was successfully treated with full-thickness anterior sclerotomy in one eye (Fig. 3).

SS-OCT findings included an elevated RPMF ($n = 9$ eyes; 75%), RPE folds ($n = 10$ eyes; 83%), retinal wrinkles ($n = 6$ eyes; 50%), and increased visibility of posterior vitreous ($n = 5$ eyes; 42%) (Fig. 3). In five eyes (42%), macular cystoid spaces of variable sizes were visible in the inner nuclear layer, with three of these eyes having additional cyst-like cavities in the ganglion cell layer. The cystoids spaces were identified within the RPMF in the five eyes and extended beyond the RPMF in two of these eyes.

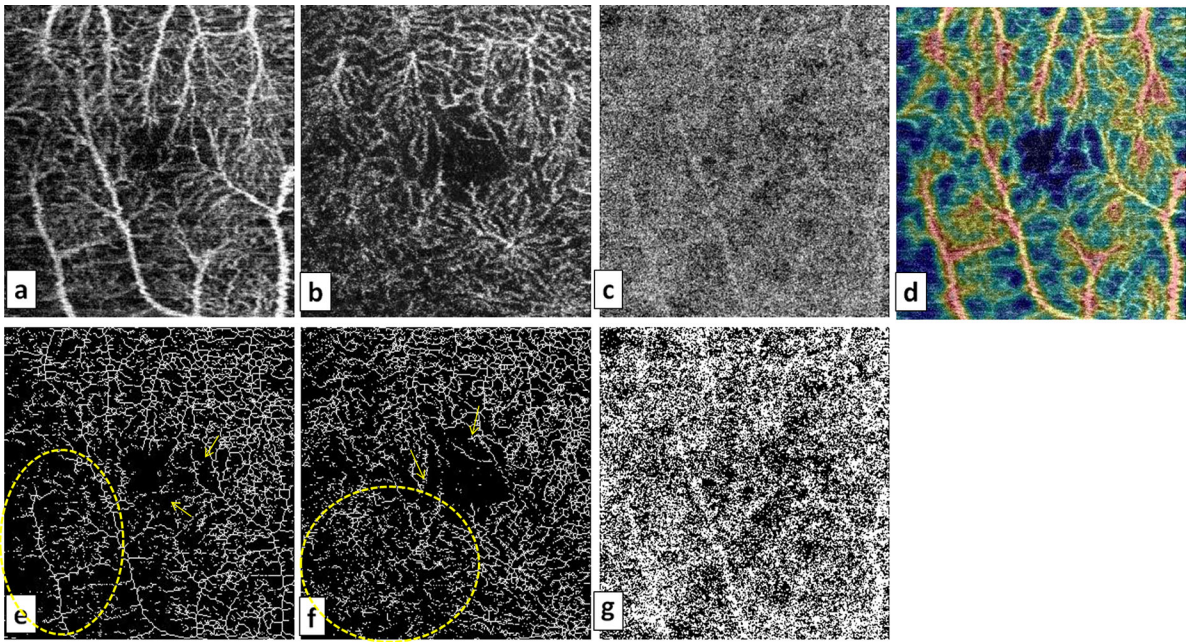

Fig. 2 3 × 3 SS-OCT angiograms of the superficial capillary plexus (**a**), deep capillary plexus (**b**) and choriocapillaris (**c**) in patient 1. The color coded OCTA map (**d**) shows clearly areas of perfusion impairment (in blue) and the perifoveal capillary changes. The corresponding skeletonized images for the capillary vessel density assessment (**e**, **f**, **g**) show area of capillary rarefaction and vessel disorganization (dashed circle), and the FAZ remodeling with vessel tortuosity, intercapillary spacing, and loss of the normal architecture of capillaries in the perifoveal area (arrows). The thresholding process of the choriocapillaris (**g**) was based on the Otsu method

Table 1 Comparison of demographic, biometric, SS-OCT, and SS-OCTA data of the two groups

Variables	PM group	Control group	*p* value
Age	42.16 ± 14.45	46.6 ± 16.36	0.413
Sex (M/F)	3/3	11/9	0.787
Global axial length (mm)	15.91 ± 0.50	23.07 ± 0.57	< 0.001
Subfoveal choroidal thickness (μm)	430.33 ± 157.48	290.05 ± 52.87	0.004
Foveal avascular zone area in the SCP (μm^2)	126.60 ± 39.76	289.35 ± 88.23	< 0.001
Foveal avascular zone area in the DCP (μm^2)	170.93 ± 39.20	308.15 ± 91.29	0.001
Capillary vessel density in the SCP (mm^{-1})	13.79 ± 1.24	14.06 ± 1.70	0.775
Capillary vessel density in the DCP (mm^{-1})	15.67 ± 0.95	17.21 ± 1.13	0.004
Capillary vessel density in the CC (mm^{-1})	48.65 ± 1.81	48.36 ± 0.59	0.726

PM posterior microphthalmos, *M* male, *F* female, *SCP* superficial capillary plexus, *DCP* deep capillary plexus, *CC* choriocapillaris

In the two eyes with clinically evident uveal effusion, SS-OCT showed subretinal fluid, multiple subretinal hyperreflective dots, and septa-like hyperreflective structures within the subretinal space (Figs. 3, 4). In one eye with large uveal effusion, the SFCT was unmeasurable preoperatively as the choroid was extremely swollen with an indistinct sclerochoroidal interface. After full-thickness anterior sclerotomy, SS-OCT showed gradual resolution of subretinal fluid with nodular RPE thickening (Fig. 3).

Mean SFCT was significantly higher in the PM group than in the control group (430.33 ± 157.48 μm vs 290.05 ± 52.87 μm; $p = 0.004$) (Table 1).

Perifoveal retinal vascular changes in SS-OCTA included FAZ remodeling with loss of the normal capillary architecture of the superficial vascular network in the perifoveal area ($n = 12$ eyes; 100%), vessel tortuosity ($n = 8$ eyes; 67%), disorganization of the deep capillary network ($n = 8$ eyes; 67%) (Figs. 2, 5), intraretinal cystoid spaces ($n = 5$ eyes; 42%)

Table 2 Demographic data and ocular features in posterior microphthalmos subjects

Patient	Age, Sex	Snellen BCVA R/L	Refractive error (*D*) R/L	Global axial length (mm) R/L	Central macular thickness (μm) R/L	Subfoveal choroidal thickness (μm) R/L	FAZ area in the SCP (μm^2) R/L	FAZ area in the DCP (μm^2) R/L	CVD in the SCP (mm^{-1}) R/L	CVD in the DCP (mm^{-1}) R/L	CVD in the CC (mm^{-1}) R/L
1	52, M	R 20/63 L 20/63	R +15.75 L +15.25	R 15.88 L 16.83	321 301	292.75 330.25	141 147.5	222 163.5	13.54 14.28	15.27 14.18	49.47 49.07
2	46, M	R 20/100 L 20/100	R +13 L +13	R 16.14 L 16.2	549 603	304.75 327.75	76.25 70	–[a] –[a]	15.67 15.24	15.32 15.22	47.35 46.14
3	40, M	R 20/200 L 20/250	R +17 L +18.75	R 15.25 L 15.10	536 594	406.5 490	97 118	–[a] –[a]	11.84 13	16.52 –[a]	47.58 –[a]
4	25, F	R 20/100 L 20/200	R +16 L +16.5	R 15.58 L 15.54	385 380	554.5 520	105 108	169 132.5	–[a] –[a]	–[a] –[a]	–[a] –[a]
5	64, F	R 20/200 L 20/200	R +15.5 L +16.5	R 16.5 L 16	318 406	253.5 333	178.5 169	172 156	12.86 13.09	16.95 16.72	46.98 52.02
6	30, F	R 20/100 L 20/400	R +17 L +18.75	R 16.2 L 15.8	301 608	555 796	114.5 194.5	124.5 225	13.21 15.18	15.24 –	49.43 49.87

M male, *F* female, *BCVA* best-corrected visual acuity, *R* right, *L* left, *FAZ* foveal avascular zone, *SCP* superficial capillary plexus, *DCP* deep capillary plexus, *CVD* capillary vessel density, *CC* choriocapillaris

[a]The missing values are related to unmeasurable FAZ area and CVD in patients due to the presence of macular cystoid spaces or subretinal fluid which may lead to an increase in image artifacts and inaccurate analysis of the CVD

(Fig. 5), capillary telangiectasia ($n = 2$ eyes; 17%) (Fig. 5), and areas of signal voids in the CC ($n = 4$ eyes; 33%) (Fig. 4).

FAZ area was measured in all eyes in the SCP OCT angiogram and only in eight eyes (67%) in the DCP one due to the presence of macular cystoid spaces or poorly defined borders of the perifoveal vascular arcade. FAZ area was significantly smaller in eyes with PM compared to the control group in both the SCP (mean 126.60 ± 39.76 μm^2 vs 289.35 ± 88.23 μm^2; $p < 0.001$) and DCP (mean 170.93 ± 39.20 μm^2 vs 308.15 ± 91.29 μm^2, $p = 0.001$) (Table 1).

The CVD was measured in 10/12 eyes (83%) in the SCP, in 8/12 eyes (66.7%) in the DCP, and 9/12 eyes (75%) in the CC. DCP-CVD in the PM group was significantly lower than in the control group ($15.67 \pm 0.95\%$ vs $17.21 \pm 1.13\%$; $p = 0.004$). There were no significant differences in CVD values in the SCP and in the CC between the two groups (Table 1).

There were significant negative correlations between SFCT with age ($r = -0.489$, $p = 0.004$), AL ($r = -0.583$, $p < 0.001$), FAZ area in the SCP ($r = -0.458$, $p = 0008$) and in the DCP ($r = -0.437$, $p = 0.002$) for the entire study population. SFCT was significantly and positively correlated with hyperopia ($r = 0.708$, $p = 0.01$) and LogMAR BCVA ($r = 0.645$, $p < 0.001$).

There were significant negative correlations between LogMAR BCVA with AL ($r = -0.929$, $p < 0.001$), FAZ area in the SCP ($r = -0.637$,

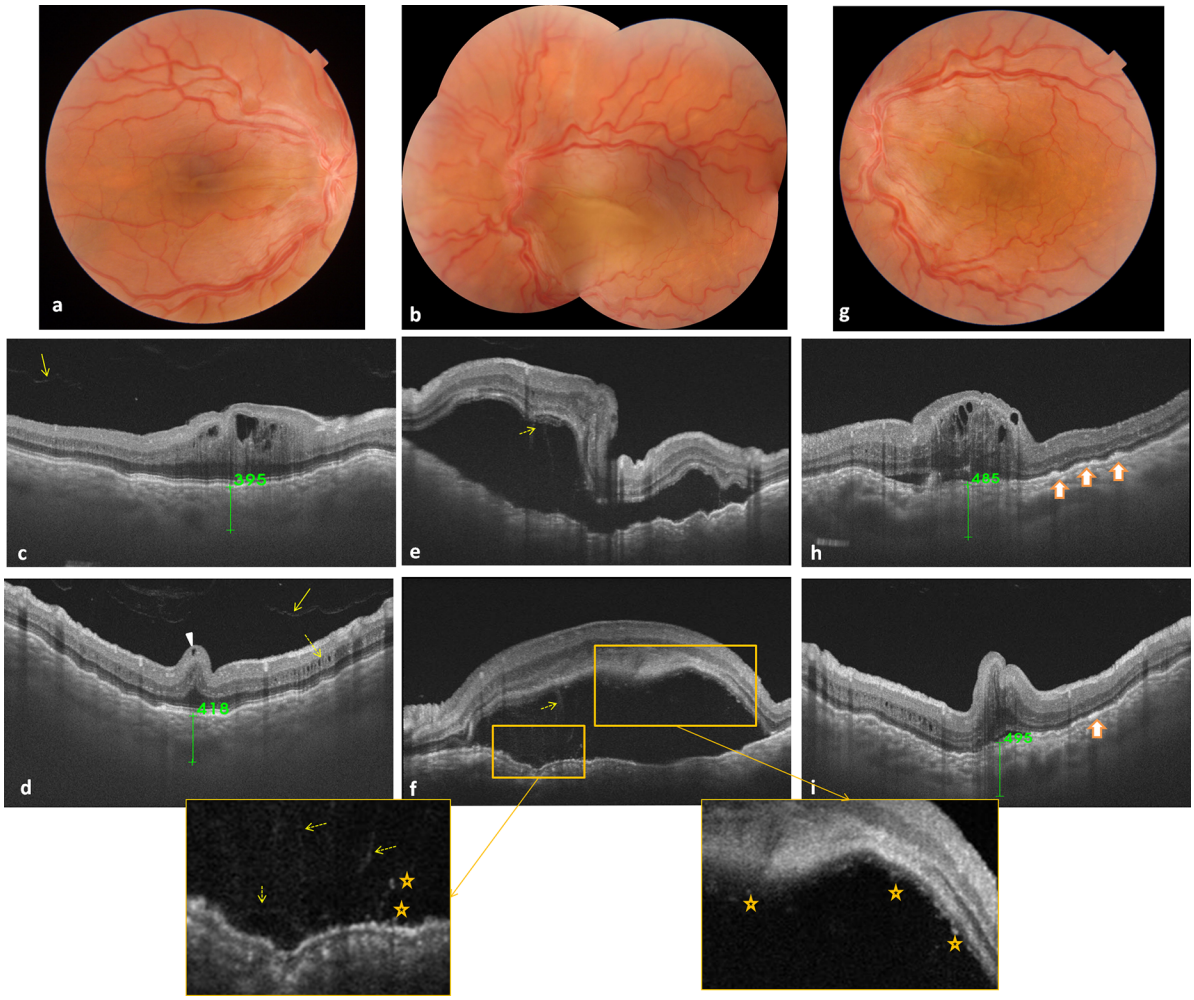

Fig. 3 (**a**, **b**) Fundus photographs OU at presentation, showing elevated RPMF and crowded optic disk with uveal effusion in the left eye. Corresponding horizontal (**c**) and vertical (**d**) SS-OCT scans at the fovea of the right eye showing increased visibility of the posterior vitreous (arrow), RPMF with cystoid cavities in the inner nuclear and ganglion cell layers (arrowhead) within and extending beyond the RPMF (dashed arrow), and a markedly thickened choroid. Horizontal (**e**) and vertical (**f**) SS-OCT scans at the fovea of the left eye showing large uveal effusion with subretinal fluid and increased RPE folds. Note the subretinal membranous structures (dashed arrow) and subretinal hyperreflective dots (star) more visible in the magnified rectangles. (**g**) Color fundus photograph of the left eye 1 month after full-thickness sclerotomy showing reattached retina. (**h**) Horizontal and (**i**) vertical SS-OCT sections at the fovea attesting resolution of the uveal effusion with residual shallow subretinal fluid, some cystoid spaces in the inner nuclear layer, and focal area of RPE thickening (full arrow)

$p < 0{,}001$) and in the DCP ($r = -0.561$, $p = 0{,}002$), and CVD in the DCP ($r = -0.450$, $p = 0.016$) for the entire study population (PM eyes and control group).

Discussion

To the best of our knowledge, the present study is the first to report the use of SS-OCT and SS-OCTA in eyes with PM. Since PM is a disorder that may affect the retina as well as the choroid, we hypothesized that the combined analysis of retina and choroid using a SS device may allow a more comprehensive evaluation of chorioretinal involvement associated with PM. This approach would also provide new insights onto the mechanisms of visual impairment in affected patients.

Our results showed that SS-OCT allows to accurately identify and characterize an array of structural changes including elevated RPMF, RPE folds, retinal wrinkles, macular cystoid spaces, subretinal fluid, and

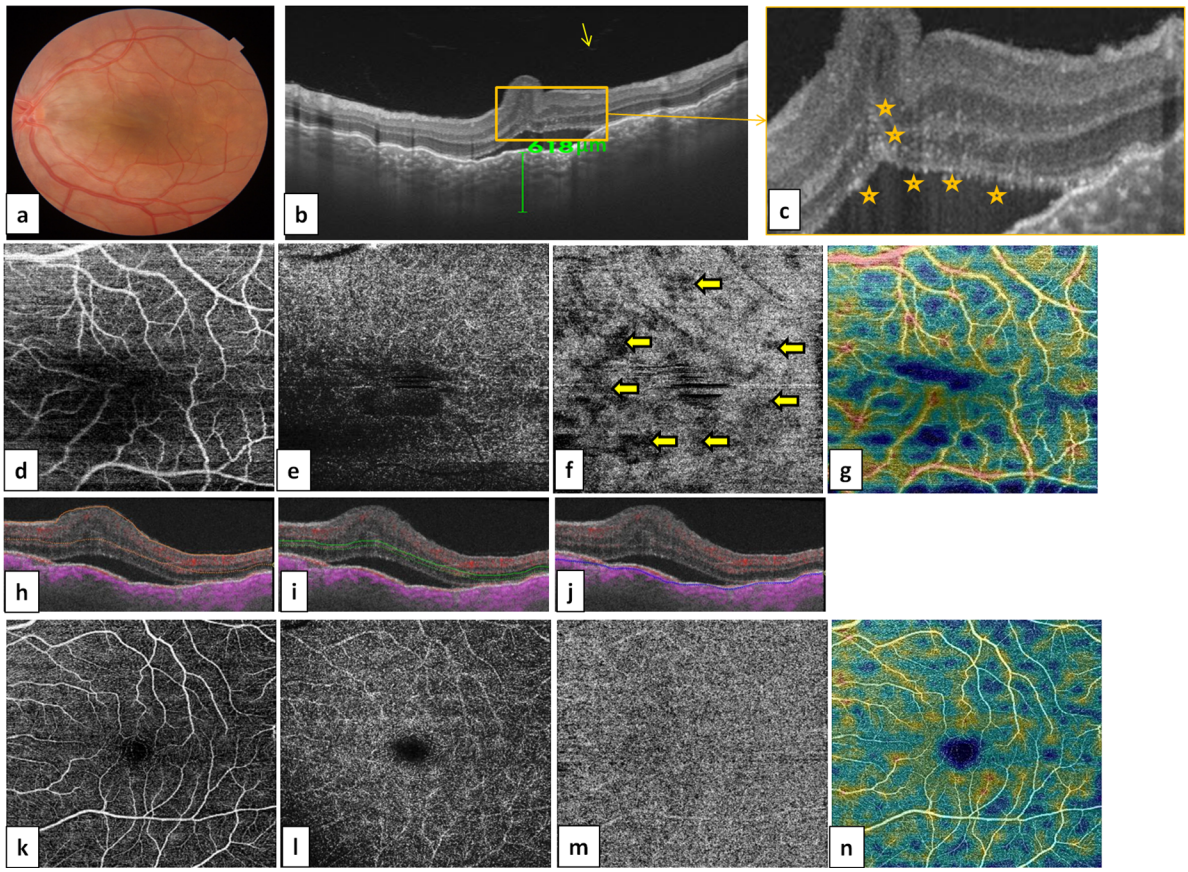

Fig. 4 Color fundus photograph (**a**), SS-OCT (**b**, **c**) and OCTA (**d**–**j**) of the left eye of the same patient in Fig. 1. (**b**) SS-OCT vertical scan shows the increased visibility of the posterior vitreous (arrow), a dome-shaped RPMF, subretinal fluid, RPE folds, and increased SFCT (618 µm). Note the subretinal hyperreflective dots (star) in the subretinal space and extending anteriorly through the RPMF more obvious in the magnified rectangle (**c**). 6 × 6 SS-OCT angiograms of the superficial capillary plexus (**d**), deep capillary plexus (**e**), choriocapillaris (**f**), and color coded OCTA map (**g**). Note the macular dragging toward the nasal area and the presence of areas of signal voids in the choriocapillaris. Corresponding OCTA B-scan with preset landmarks of the segmentation between which the patterns of the capillary plexuses were recorded (**h**, **i**, **j**). 6 × 6 SS-OCT angiograms of the superficial capillary plexus (**k**), deep capillary plexus (**l**), choriocapillaris (**m**), and color coded OCTA map (**n**) in an age-matched subject

increased visibility of posterior vitreous. These results are consistent with those from previous SD-OCT studies [5, 7–10] reporting intraretinal cystoid spaces involving the RPMF. As previously reported using SD-OCT [5, 7], as well as in our subset of patients, intraretinal cystoid spaces involving the RPMF area were identified. However, in the current study, due to the capability of SS-OCT to acquire wide-field scans, we highlighted that the cystoid spaces extended beyond the RPMF area.

SS-OCT showed in two eyes a serous macular retinal detachment as a probable consequence of uveal effusion that was associated with multiple subretinal hyperreflective dots and barely visible septa-like structures. Such findings have not been reported in previous SD-OCT studies on PM. Such abnormal subretinal findings might correspond to a fibrinous or proteinaceous subretinal material from the choroidal vasculature through marked breakdown of the outer blood–retinal barrier at the RPE level. Alternatively, they might represent a portion of the outer segment photoreceptor layer that was separated from the inner segment layer by subretinal fluid.

The results of our study showed that SFCT was significantly higher in the PM group than in the control group. Demircan et al. [16] reported similar results in

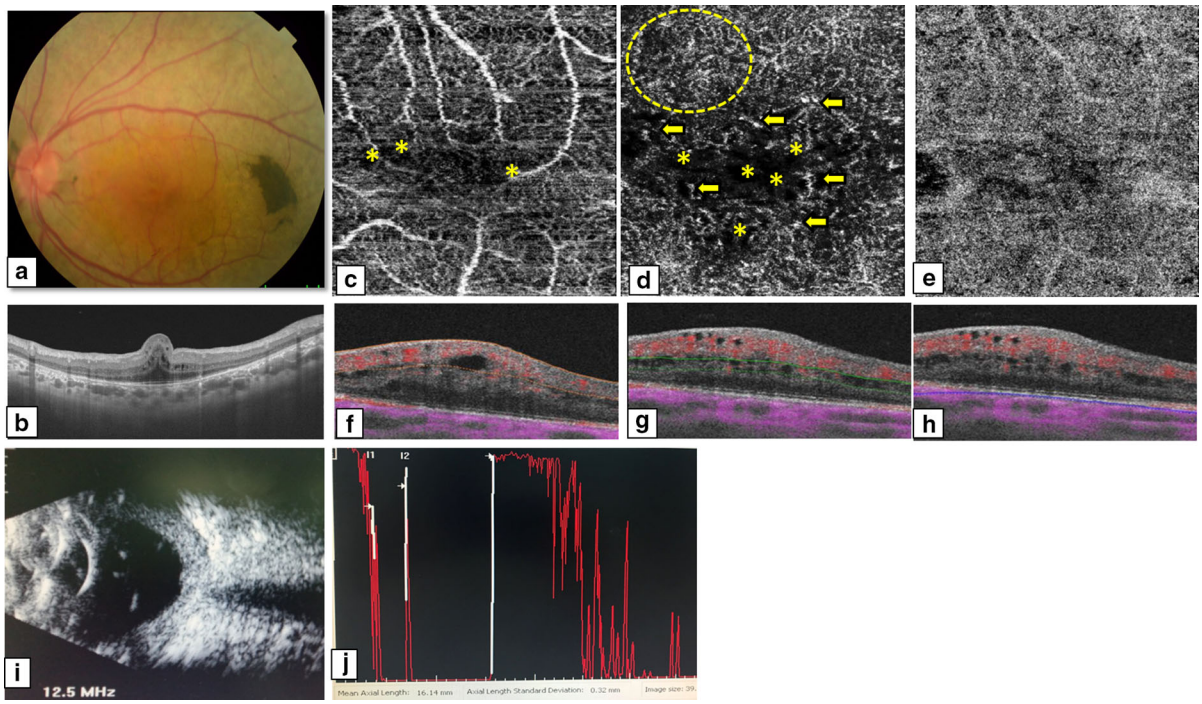

Fig. 5 (**a**) Color fundus photograph of the left eye of patient 2 shows a crowded optic disk with retinal pigmentary changes. (**b**) SS-OCT vertical scan shows a dome-shaped RPMF, and cystoid cavities in the inner nuclear layer. The 3 × 3 SS-OCTA reveals at the level of the superficial capillary plexus (**c**) FAZ remodeling with loss of the normal capillary architecture with some capillaries crossing the fovea, and some well-defined black, roundish areas corresponding to intraretinal cystoids spaces (yellow star). OCTA of the deep capillary plexus (**d**) shows large areas of capillary rarefaction and network disorganization (yellow dashed lines) with numerous cystoid spaces (yellow star) with some focal vascular dilatations (full arrow). (**e**) OCTA of the choriocapillaris shows the presence of signal voids. (**f**, **g**, **h**) The co-registered OCTA B-scan clearly shows the presence of cystoid spaces at the level of the superficial ad deep capillary plexuses. (**i**) B-scan ultrasonography shows a foreshortening of the vitreous cavity and sclerochoroidal thickening. (**j**) The total AL was 16.14 mm

nanophthalmic eyes using EDI-OCT. Previous studies showed that SS-OCT provides a better visualization of the choroid and the sclerochoroidal boundary compared to the SD-OCT (and even than EDI-OCT) both in normal and diseased eyes [17–20]. A choroidal thickening might indicate choroidal vascular hyperpermeability and increased hydrostatic pressure in the choroid. The increased resistance to both protein movement and venous outflow through the abnormal sclera may result in choroidal thickening and congestion, folding at the inner choroidal surface and subsequent uveal effusion, as seen in two of our patients [21]. Alternatively, the abnormal sclera in PM and nanophthalmic eyes might compress the vortex vein and lead to choroidal congestion [22]. Thus, RPMF may be secondary to a disparity in growth between the sclera and retina.

The sclerotomy we successfully performed to treat the patient with extensive uveal effusion have previously been found to be effective in managing patients with idiopathic uveal effusion syndrome and nanophthalmos [23, 24].

Thanks to SS-OCTA, a wide variety of retinal microvascular changes involving the SCP and/or DCP were detected in our patients with PM. These included FAZ remodeling, significant FAZ area reduction, capillary network disorganization, capillary telangiectasia, intraretinal cystoid spaces, and capillary rarefaction in the DCP.

Although the absence or a marked reduction of FAZ area has been previously described in eyes with PM using FA [3, 4], this is the first OCTA-based quantitative FAZ assessment. In addition, the loss of the normal capillary architecture in the perifoveal area with increased intercapillary spacing as shown by SS-

OCTA suggests that the foveal vasculature might be poorly differentiated in PM eyes. Recent studies using OCTA showed that FAZ attenuation, capillary tortuosity, foveal folds, and thickened subfoveal choroid characterize the nanophthalmic eyes [25, 26]. Thus, quantitative and qualitative capillary changes detected by SS-OCTA in PM eyes might indicate an underdevelopment of foveal vasculature.

In the current study, a significant reduction in DCP-CVD was reported in the PM group compared to the control group, whereas there was no significant difference in the CVD in the SCP between the two groups. This quantitative data are consistent with the qualitative findings (i.e., disorganization of the DCP, intraretinal cystoid spaces, and capillary telangiectasia). It might be speculated that the DCP, as it is positioned in a watershed-like region, could be more vulnerable and therefore easily affected by the pathological process compared to the SCP. In addition, the presence of cystoid spaces in the inner nuclear layer, where the DCP is located, confirms the potential perfusion impairment of the DCP in PM eyes and thus reflects the significant correlation between structural and functional (perfusion) abnormalities.

Moreover, in this study, areas of signal voids were seen in the CC in a subset of PM eyes. This might indicate microvascular flow deficits, which could originate from mechanical compression induced by an abnormal thickened sclerochoroid. Nevertheless, there was no significant difference in the CVD in the CC between the two groups.

The results of our study, consistent with those of previous studies, showed a negative correlation between SFCT with AL and age [15, 27, 28]. Interestingly, we also found that SFCT negatively and significantly correlated with both superficial and deep FAZ area in all studied group. We might therefore argue that as the eye gets shorter, SFCT increases, and FAZ area decreases.

Additionally, data from our study showed a significant negative correlation between Log MAR BCVA with AL, FAZ area, and CVD in the DCP. Although high hyperopia, elevated RPMF, and uveal effusion are the main causes of visual impairment, other microvascular changes, accurately reflected by OCTA, could be a further cause of visual disturbance in these eyes. We might postulate that these vascular changes might be induced by a combination of structural changes of the sclera, pathological thickening of the choroid, and dysgenesis of the perifoveal vascular architecture.

There are several limitations in our study. The most significant concerns with OCTA images are image artifacts and segmentation failure in PM eyes. Two eyes of our patients with SRF, which may lead to an increase in image artifacts, were excluded from the vessel density analysis. Intrinsic characteristics of these shorter and abnormally posteriorly shaped eyes may lead to defects in images analyzing. Additionally, an accurate analysis of OCTA images in patients with a low BCVA compared with patients with a good BCVA could be difficult because of an unstable gaze. Although aware of these limitations, the considerable and consistent differences in OCTA measurements between PM and control eyes were, however, higher than what could be attributed to the effect of such potential confounders.

In conclusion, data from our study provide an objective comprehensive evaluation of retinal and choroidal changes in PM eyes using SS-OCT and SS-OCTA. These noninvasive imaging modalities may prove clinically useful in evaluating chorioretinal structural and microvascular involvement in eyes with PM, leading to a further understanding of visual disturbance in these patients.

Acknowledgements This work has been supported by the Ministry of Higher Education and Research of Tunisia.

Compliance with ethical standards

Conflict of interest The authors declare that they have no conflict of interest.

Ethical approval All procedures performed in studies involving human participants were in accordance with the ethical standards of the institutional and/or national research committee and with the 1964 Helsinki declaration and its later amendments or comparable ethical standards.

Informed consent Informed consent was obtained from all individual participants included in the study.

References

1. Spitznas M, Gerke E, Bateman VB (1983) Hereditary posterior microphthalmos with papillomacular fold and high hyperopia. Arch Ophthalmol 101:413–417
2. Boynton JR, Purnell EW (1975) Bilateral microphthalmos without microcornea associated with unusual

papillomacular retinal folds and high hyperopia. Am J Ophthalmol 79:820–826
3. Khairallah M, Messaoud R, Zaouali S, Ben Yahia S, Ladjimi A, Jenzri S (2002) Posterior segment changes associated with posterior microphthalmos. Ophthalmology 109:569–574
4. Walsh MK, Goldberg MF (2007) Abnormal foveal avascular zone in nanophthalmos. Am J Ophthalmol 143:1067–1068
5. Nowilaty SR, Mousa A, Ghazi NG (2013) The posterior pole and papillomacular fold in posterior microphthalmos: novel spectral-domain optical coherence tomography findings. Ophthalmology 120:1656–1664
6. Nowilaty SR, Khan AO, Aldahmesh MA, Tabbara KF, Al-Amri A, Alkuraya FS (2013) Biometric and molecular characterization of clinically diagnosed posterior microphthalmos. Am J Ophthalmol 155:361–372.e7
7. Jackson TE, Yang YC, Shun-Shin GA (2012) Spectral domain optical coherence tomography findings in retinal folds associated with posterior microphthalmos. J AAPOS 16:389–391
8. Aras C, Ozdamar A, Ustundag C, Ozkan S (2005) Optical coherence tomographic features of papillomacular fold in posterior microphthalmos. Retina 25:665–667
9. Kumar M, Das T, Kesarwani S (2012) Spectral domain optical coherence tomography finding in posterior microphthalmos. Clin Exp Optom 95:651–652
10. Liu JJ, Chen YY, Zhang X, Zhao PQ (2018) Clinical features of posterior microphthalmic and nanophthalmic eyes. Int J Ophthalmol 11:1829–1834
11. Spaide RF, Fujimoto JG, Waheed NK, Sadda SR, Staurenghi G (2018) Optical coherence tomography angiography. Prog Retin Eye Res 64:1–55
12. Kim AY, Chu Z, Shahidzadeh A, Wang RK, Puliafito CA, Kashani AH (2016) Quantifying microvascular density and morphology in diabetic retinopathy using spectral-domain optical coherence tomography angiography. Invest Ophthalmol Vis Sci 57:OCT362–OCT370
13. Pichi F, Sarraf D, Arepalli S et al (2017) The application of optical coherence tomography angiography in uveitis and inflammatory eye diseases. Prog Retin Eye Res 59:178–201
14. Otsu N (1979) A threshold selection method from gray-level histograms. IEEE Trans Syst Man Cybern 9:62–66
15. Al-Sheikh M, Phasukkijwatana N, Dolz-Marco R et al (2017) Quantitative OCT angiography of the retinal microvasculature and the choriocapillaris in myopic eyes. Invest Ophthalmol Vis Sci 58:2063–2069
16. Demircan A, Altan C, Osmanbasoglu OA et al (2014) Subfoveal choroidal thickness measurements with enhanced depth imaging optical coherence tomography in patients with nanophthalmos. Br J Ophthalmol 98:345–349
17. Matsuo Y, Sakamoto T, Yamashita T et al (2013) Comparisons of choroidal thickness of normal eyes obtained by two different spectral-domain OCT instruments and one swept-source OCT instrument. Invest Ophthalmol Vis Sci 54:7630–7636
18. Ikuno Y, Maruko I, Yasuno Y et al (2011) Reproducibility of retinal and choroidal thickness measurements in enhanced depth imaging and high-penetration optical coherence tomography. Invest Ophthalmol Vis Sci 52:5536–5540
19. Tan CS, Ngo WK, Cheong KX (2015) Comparison of choroidal thicknesses using swept source and spectral domain optical coherence tomography in diseased and normal eyes. Br J Ophthalmol 99:354–358
20. Chee SP, Chan SN, Jap A (2017) Comparison of enhanced depth imaging and swept source optical coherence tomography in assessment of choroidal thickness in Vogt–Koyanagi–Harada disease. Ocul Immunol Inflamm 25:528–532
21. Brockhurst RJ (1975) Nanophthalmos with uveal effusion. A new clinical entity. Arch Ophthalmol 93:1989–1999
22. Gass JD (1983) Uveal effusion syndrome: a new hypothesis concerning pathogenesis and technique of surgical treatment. Trans Am Ophthalmol Soc 81:246–260
23. Faulborn J, Kölli H (1999) Sclerotomy in uveal effusion syndrome. Retina 19:504–507
24. Kong M, Kim JH, Kim SJ, Kang SW (2013) Full-thickness sclerotomy for uveal effusion syndrome. Korean J Ophthalmol 27:294–298
25. Demircan A, Yesilkaya C, Altan C, Alkin Z, Yasa D, Aygit ED, Bektasoglu D (2018) Foveal avascular zone area measurements with optical coherence tomography angiography in patients with nanophthalmos. Eye (Lond). https://doi.org/10.1038/s41433-018-0236-7
26. Mansour AM, Stewart MW, Yassine SW et al (2018) Unmeasurable small size superficial and deep foveal avascular zone in nanophthalmos: the Collaborative Nanophthalmos OCTA Study. Br J Ophthalmol. https://doi.org/10.1136/bjophthalmol-2018-312781
27. Wei WB, Xu L, Jonas JB et al (2013) Subfoveal choroidal thickness: the Beijing Eye Study. Ophthalmology 120:175–180
28. Ikuno Y, Kawaguchi K, NouchiT Yasuno Y (2010) Choroidal thickness in healthy Japanese subjects. Invest Ophthalmol Vis Sci 51:2173–2176